

A Search for Nucleon Decay via $n \rightarrow \bar{\nu}\pi^0$ and $p \rightarrow \bar{\nu}\pi^+$ in Super-Kamiokande

K. Abe,^{1,27} Y. Hayato,^{1,27} T. Iida,¹ K. Iyogi,¹ J. Kameda,^{1,27} Y. Koshio,^{1,27} Y. Kozuma,¹ Ll. Marti,¹ M. Miura,^{1,27} S. Moriyama,^{1,27} M. Nakahata,^{1,27} S. Nakayama,^{1,27} Y. Obayashi,^{1,27} H. Sekiya,^{1,27} M. Shiozawa,^{1,27} Y. Suzuki,^{1,27} A. Takeda,^{1,27} Y. Takenaga,¹ K. Ueno,¹ K. Ueshima,¹ S. Yamada,¹ T. Yokozawa,¹ C. Ishihara,² H. Kaji,² T. Kajita,^{2,27} K. Kaneyuki,^{2,27,*} K.P. Lee,² T. McLachlan,² K. Okumura,² Y. Shimizu,² N. Tanimoto,² L. Labarga,³ E. Kearns,^{4,27} M. Litos,⁴ J.L. Raaf,⁴ J.L. Stone,^{4,27} L.R. Sulak,⁴ M. Goldhaber,^{5,*} K. Bays,⁶ W.R. Kropp,⁶ S. Mine,⁶ C. Regis,⁶ A. Renshaw,⁶ M.B. Smy,^{6,27} H.W. Sobel,^{6,27} K.S. Ganezer,⁷ J. Hill,⁷ W.E. Keig,⁷ J.S. Jang,^{8,†} J.Y. Kim,⁸ I.T. Lim,⁸ J.B. Albert,⁹ K. Scholberg,^{9,27} C.W. Walter,^{9,27} R. Wendell,⁹ T.M. Wongjirad,⁹ T. Ishizuka,¹⁰ S. Tasaka,¹¹ J.G. Learned,¹² S. Matsuno,¹² S.N. Smith,¹² T. Hasegawa,¹³ T. Ishida,¹³ T. Ishii,¹³ T. Kobayashi,¹³ T. Nakadaira,¹³ K. Nakamura,^{13,27} K. Nishikawa,¹³ Y. Oyama,¹³ K. Sakashita,¹³ T. Sekiguchi,¹³ T. Tsukamoto,¹³ A.T. Suzuki,¹⁴ Y. Takeuchi,^{14,27} M. Ikeda,¹⁵ A. Minamino,¹⁵ T. Nakaya,^{15,27} Y. Fukuda,¹⁶ Y. Itow,^{17,18} G. Mitsuka,¹⁷ T. Tanaka,¹⁷ C.K. Jung,¹⁹ G.D. Lopez,¹⁹ I. Taylor,¹⁹ C. Yanagisawa,¹⁹ H. Ishino,²⁰ A. Kibayashi,²⁰ S. Mino,²⁰ T. Mori,²⁰ M. Sakuda,²⁰ H. Toyota,²⁰ Y. Kuno,²¹ M. Yoshida,²¹ S.B. Kim,²² B.S. Yang,²² H. Okazawa,²³ Y. Choi,²⁴ K. Nishijima,²⁵ M. Koshihara,²⁶ M. Yokoyama,^{26,27} Y. Totsuka,^{26,*} K. Martens,²⁷ J. Schuemann,²⁷ M.R. Vagins,^{27,6} S. Chen,²⁸ Y. Heng,²⁸ Z. Yang,²⁸ H. Zhang,²⁸ D. Kielczewska,²⁹ P. Mijakowski,²⁹ K. Connolly,³⁰ M. Dziomba,³⁰ E. Thrane,^{30,‡} and R.J. Wilkes³⁰

(The Super-Kamiokande Collaboration)

¹Kamioka Observatory, Institute for Cosmic Ray Research, University of Tokyo, Kamioka, Gifu 506-1205, Japan

²Research Center for Cosmic Neutrinos, Institute for Cosmic Ray Research, University of Tokyo, Kashiwa, Chiba 277-8582, Japan

³Department of Theoretical Physics, University Autonoma Madrid, 28049 Madrid, Spain

⁴Department of Physics, Boston University, Boston, MA 02215, USA

⁵Physics Department, Brookhaven National Laboratory, Upton, NY 11973, USA

⁶Department of Physics and Astronomy, University of California, Irvine, Irvine, CA 92697-4575, USA

⁷Department of Physics, California State University, Dominguez Hills, Carson, CA 90747, USA

⁸Department of Physics, Chonnam National University, Kwangju 500-757, Korea

⁹Department of Physics, Duke University, Durham NC 27708, USA

¹⁰Junior College, Fukuoka Institute of Technology, Fukuoka, 811-0214, Japan

¹¹Information and Multimedia Center, Gifu University, Gifu, Gifu 501-1193, Japan

¹²Department of Physics and Astronomy, University of Hawaii, Honolulu, HI 96822, USA

¹³High Energy Accelerator Research Organization (KEK), Tsukuba, Ibaraki 305-0801, Japan

¹⁴Department of Physics, Kobe University, Kobe, Hyogo 657-8501, Japan

¹⁵Department of Physics, Kyoto University, Kyoto 606-8502, Japan

¹⁶Department of Physics, Miyagi University of Education, Sendai, Miyagi 980-0845, Japan

¹⁷Solar Terrestrial Environment Laboratory, Nagoya University, Nagoya, Aichi 464-8602, Japan

¹⁸Kobayashi-Maskawa Institute for the Origin of Particles and the Universe, Nagoya University, Nagoya, Aichi 464-8602, Japan

¹⁹Department of Physics and Astronomy, State University of New York, Stony Brook, NY 11794-3800, USA

²⁰Department of Physics, Okayama University, Okayama, Okayama 700-8530, Japan

²¹Department of Physics, Osaka University, Toyonaka, Osaka 560-0043, Japan

²²Department of Physics, Seoul National University, Seoul 151-742, Korea

²³Department of Informatics in Social Welfare, Shizuoka University of Welfare, Yaizu, Shizuoka, 425-8611, Japan

²⁴Department of Physics, Sungkyunkwan University, Suwon 440-746, Korea

²⁵Department of Physics, Tokai University, Hiratsuka, Kanagawa 259-1292, Japan

²⁶The University of Tokyo, Bunkyo, Tokyo 113-0033, Japan

²⁷Kavli Institute for the Physics and Mathematics of the Universe (WPI), Todai Institutes for Advanced Study, University of Tokyo, Kashiwa, Chiba 277-8583, Japan

²⁸Department of Engineering Physics, Tsinghua University, Beijing, 100084, China

²⁹Institute of Experimental Physics, Warsaw University, 00-681 Warsaw, Poland

³⁰Department of Physics, University of Washington, Seattle, WA 98195-1560, USA

(Dated: November 7, 2018)

We present the results of searches for nucleon decay via $n \rightarrow \bar{\nu}\pi^0$ and $p \rightarrow \bar{\nu}\pi^+$ using data from a combined 172.8 kton · years exposure of Super-Kamiokande-I, -II, and -III. We set lower limits on the partial lifetime for each of these modes: $\tau_{n \rightarrow \bar{\nu}\pi^0} > 1.1 \times 10^{33}$ years and $\tau_{p \rightarrow \bar{\nu}\pi^+} > 3.9 \times 10^{32}$ years at 90% confidence level.

PACS numbers: 13.30.-a, 11.30.Fs, 12.60.Jv, 14.20.Dh, 29.40.Ka

Although there is strong theoretical support that nature can be described by a grand unified theory (GUT) [1, 2], there is currently no direct experimental evidence. One of the most powerful ways to test grand unification is to look for proton (or bound neutron) decay. Most GUTs have an unstable proton; in the absence of an observation, setting experimental limits on the proton lifetime can provide useful constraints on the nature of grand unified theories. Observation, on the other hand, would be tantalizing evidence of new physics beyond the Standard Model.

One of the more simple but interesting candidates for grand unification is SO(10), where the Standard Model's SU(3), SU(2), and U(1) are contained within the larger gauge group. The class of models based on SO(10) unification generally make predictions for neutrino masses and mixing that are broadly in accord with all known neutrino mixing data [3, 4]. The minimal supersymmetric SO(10) model with a **126** Higgs field described in Ref. [3] is the particular motivation for the analysis presented here. In addition to predicting neutrino mass and mixing in agreement with observations, it leaves R-parity unbroken, which guarantees the existence of stable dark matter. For some region of its allowed parameter space, this model predicts that the dominant nucleon decay modes will be $p \rightarrow \bar{\nu}\pi^+$ and $n \rightarrow \bar{\nu}\pi^0$.

In this Letter, the fully-contained (FC) atmospheric neutrino data (*i.e.*, having activity only within the inner detector region and no activity in the outer detector) collected during the first three running periods of Super-Kamiokande (Super-K, SK) are analyzed in a search for both $p \rightarrow \bar{\nu}\pi^+$ and $n \rightarrow \bar{\nu}\pi^0$: SK-I (May 1996–Jul 2001, 1489.2 live days), SK-II (Jan 2003–Oct 2005, 798.6 live days), and SK-III (Sep 2006–Aug 2008, 518.1 live days). The combined dataset corresponds to an exposure of 172.8 kton \cdot yrs.

The 50-kiloton (22.5 kton fiducial) Super-K water Cherenkov detector is located beneath 1 km of rock overburden (2700 meters water equivalent) in the Kamioka mine in Japan. Details of the detector design, calibration, and simulations in SK-I may be found in Ref. [5] and a discussion of the reduced photo-sensor coverage in SK-II may be found in Ref. [6]. In SK-III, the photo-sensor coverage is recovered to the original 40% level of SK-I.

The efficiency of detecting nucleon decay occurring in the water is estimated by Monte Carlo (MC) simulation. As discussed in detail in Ref. [6], all nucleons in the H₂O molecule are assumed to decay with equal probability, and Fermi motion, nuclear binding energy, and meson-nuclear interactions in oxygen are taken into account.

The $n \rightarrow \bar{\nu}\pi^0$ ($p \rightarrow \bar{\nu}\pi^+$) decay mode results in a π^0 (π^+) with mean momentum 460 MeV/ c (458.8 MeV/ c), smeared by the Fermi motion of nucleons bound in oxygen, but uniquely determined for decays of the two free protons in the water's hydrogen nuclei. The pion's mo-

mentum is also affected by nuclear interactions as it travels through the nucleus; it may undergo scattering, charge exchange, or absorption. Pion-nucleon interactions are carefully simulated to reflect our understanding of the processes which may affect the ability to detect pions in water.

Since the final state neutrino is undetected, these two modes of nucleon decay are particularly challenging. It is not possible to develop a set of selection cuts that will eliminate most of the background of atmospheric neutrino interactions with a single pion and no other detected particles in the final state. Instead, we select events that appear to have only a single π^0 or π^+ , and perform a spectrum fit to their reconstructed momentum distributions, respectively. In this method, the nearly mono-energetic pions from nucleon decay would appear as a bump on top of the broad distribution of pions from atmospheric neutrino interactions. Atmospheric neutrino background events are simulated using the NEUT neutrino interaction MC simulation [7] with an atmospheric neutrino flux calculated by Honda *et al.* [8], then passed through a GEANT-3-based [9] custom detector simulation that is described in detail in Ref. [10].

The event selection cuts applied to the fully-contained atmospheric neutrino data are: (A) the number of Cherenkov rings is two for $n \rightarrow \bar{\nu}\pi^0$ (one for $p \rightarrow \bar{\nu}\pi^+$), (B) all rings are showering (electron-like) for $n \rightarrow \bar{\nu}\pi^0$ (non-showering (muon-like) for $p \rightarrow \bar{\nu}\pi^+$), (C) the number of electrons from muon decay is zero for $n \rightarrow \bar{\nu}\pi^0$ (zero or one for $p \rightarrow \bar{\nu}\pi^+$), and (D) the reconstructed momentum is less than 1000 MeV/ c . For the $n \rightarrow \bar{\nu}\pi^0$ sample only, there is one additional requirement (E) that the reconstructed invariant mass of the π^0 is between 85 MeV/ c^2 and 185 MeV/ c^2 . A discussion of the momentum reconstruction and performance can be found in Refs. [6, 11]. The selected fraction of single pions in the atmospheric neutrino MC with these cuts are shown as a function of reconstructed momentum for SK-I in Fig. 1(a) for π^0 , and 1(b) for π^+ . The efficiency curves for the SK-II and SK-III periods, not shown here but treated individually in the fit, are very similar to the SK-I curves shown in the figure. For the π^0 mode, the majority of atmospheric neutrino-induced background events that pass the selection cuts arise from neutral current (NC) single pion production (76%). The other backgrounds are due to charged current (CC) single pion production with the outgoing charged lepton below Cherenkov threshold (7%), NC multiple pion production (7%), and small fractions of other processes (less than a few percent each). As this background is overwhelmingly made up of pions and their selection efficiency as a function of momentum is not flat, the uncertainty in selection efficiency is treated as a systematic error binned in momentum. Efficiency is defined as the fraction of all fully-contained events in the fiducial volume (FCFV) with at least one π^0 and no decay electrons, which pass the selection cuts for $n \rightarrow \bar{\nu}\pi^0$. For

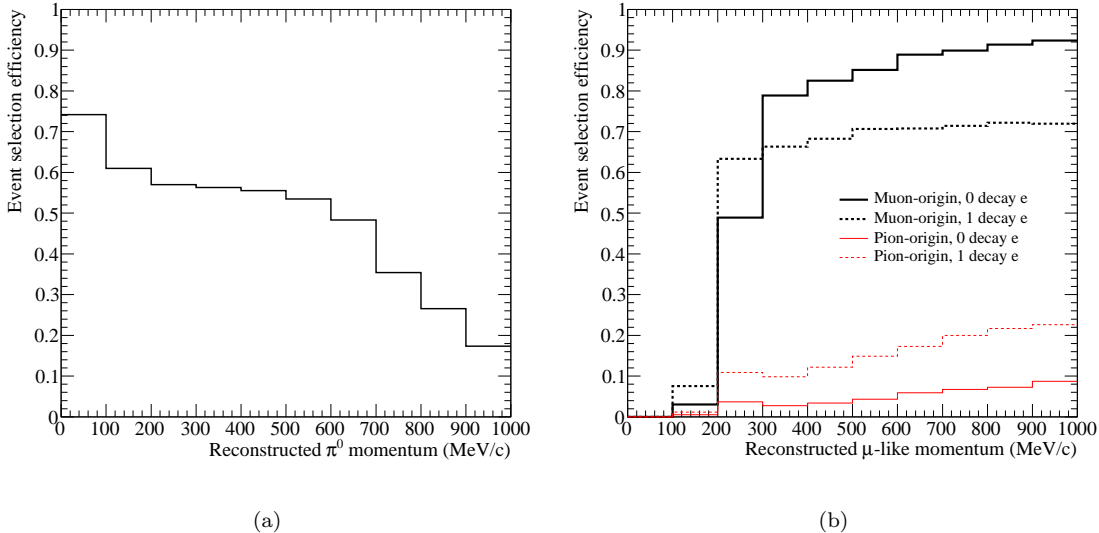


FIG. 1: Event selection efficiencies for atmospheric neutrino MC as a function of reconstructed momentum for (a) $n \rightarrow \bar{\nu}\pi^0$ selection cuts and (b) $p \rightarrow \bar{\nu}\pi^+$ selection cuts. For the π^+ sample, all momenta are calculated assuming a muon hypothesis. The atmospheric neutrino events that make up the background for the $p \rightarrow \bar{\nu}\pi^+$ mode are treated separately in the spectrum fit according to their origin.

the π^+ sample, a large fraction of the background events are of non-pionic origin, as shown in the first row of Table I. Since the shape and level of the selection efficiency differs for backgrounds of pionic and muonic origin, as demonstrated in Fig. 1(b), these two cases are treated as separate systematic errors in the spectrum fit. Efficiency curves in this case are calculated using the MC truth neutrino interaction mode in the denominator to determine what fraction of events pass the $p \rightarrow \bar{\nu}\pi^+$ selection cuts for: (1) FCFV events which originate from charged current quasi-elastic interactions (muonic origin), and (2) FCFV events which originate from interactions that truly have a π^+ (pionic origin).

TABLE I: Sources of atmospheric neutrino- and antineutrino-induced background for the $p \rightarrow \bar{\nu}\pi^+$ decay mode.

Interaction mode	Fraction of background
CCQE ($\nu n \rightarrow \mu p$)	0.75
Single- π ($\nu N \rightarrow \ell N' \pi^{(+/-/0)}$)	0.20
Multi- π ($\nu N \rightarrow \ell N' (n\pi)$)	0.03
Other	0.02

The SK particle identification (PID) algorithm only classifies Cherenkov rings as showering (e^\pm, γ) or non-showering (μ^\pm, π^\pm), as described in Ref. [10]. Another PID algorithm which uses additional information about the Cherenkov ring opening angle to attempt further classification between μ and π^\pm rings also exists [6], but was shown to add no improvement to this analysis; thus, no attempt is made to separate muon-induced rings from pion-induced rings.

The fit to the reconstructed momentum spectrum is a χ^2 minimization based on a Poisson probability with systematic errors taken into account by quadratic penalties (pull terms). This technique is the same as that described by Fogli *et al.*, in Ref. [12]. The χ^2 is defined as

$$\chi^2 = 2 \sum_{i=1}^{\text{nbins}} \left(N_i^{\text{exp}} \left(1 + \sum_{j=1}^{N_{\text{syserr}}} f_i^j \epsilon_j \right) - N_i^{\text{obs}} \right) + N_i^{\text{obs}} \ln \frac{N_i^{\text{obs}}}{N_i^{\text{exp}} \left(1 + \sum_{j=1}^{N_{\text{syserr}}} f_i^j \epsilon_j \right)} + \sum_{j=1}^{N_{\text{syserr}}} \left(\frac{\epsilon_j}{\sigma_j} \right)^2, \quad (1)$$

where i indexes the data bins, N_i^{exp} is the MC expectation, and N_i^{obs} is the number of observed events in the i^{th} bin. The Monte Carlo simulation expectation is given by $N_i^{\text{exp}} = \alpha \cdot N_i^{\text{bkg}} + \beta \cdot N_i^{\text{sig}}$, where α and β are the normalization parameters for background (atmospheric neutrinos) and signal (nucleon decay), respectively. In the two-dimensional fit space, the parameter allowed ranges are defined such that a value of 1.0 for α (atmospheric neutrino background normalization) and a value of 0.0 for β (nucleon decay signal event normalization) would indicate that the SK data are perfectly described by the atmospheric neutrino simulation alone, with no contribution from nucleon decay. The effect of the j^{th} systematic error is included via a “pull term” which includes the error parameter ϵ_j and f_i^j , which is the fractional change in the MC expectation for bin i that would occur for a 1-

sigma change in systematic error σ_j . In total, 30 bins are used to compute the value of χ^2 for the $n \rightarrow \bar{\nu}\pi^0$ analysis (10 for SK-I, 10 for SK-II, and 10 for SK-III), and 60 bins are used for the $p \rightarrow \bar{\nu}\pi^+$ analysis. The number of bins in the π^+ analysis is double that of the π^0 analysis due to the presence of two independent subsamples (events with zero and one decay electron, respectively) in the selected data for that decay mode.

Equation 1 is minimized with respect to the ϵ_j according to $\partial\chi^2/\partial\epsilon_j = 0$, which yields a set of iteratively solved equations in the epsilons. The χ^2 is calculated by this procedure for 10,000 points in the fit parameter space ($\alpha : [0.8, 1.2], \beta : [0.0, 0.2]$). Each SK run period uses an independent sample of 500 years of atmospheric neutrino MC simulation, and an independent sample of 5000 events of the pertinent nucleon decay MC simulation to calculate N_i^{exp} . The global minimum χ^2 for each decay mode is defined as that decay mode's best fit point.

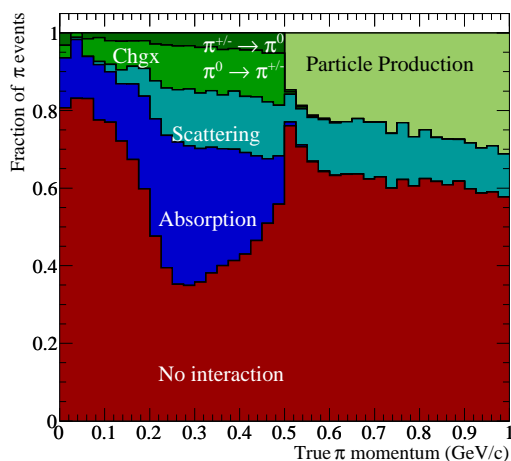


FIG. 2: Cumulative fractions of nuclear effects for π^0 as a function of true π^0 momentum for atmospheric neutrino interactions. The fractions of events which undergo charge exchange, multiple particle production, scattering, and absorption are shown by various shades as labeled. Pions which exit the nucleus without experiencing any nuclear effect are indicated by the portion labeled “No interaction.”

Six sources of systematic uncertainty are considered in the $n \rightarrow \bar{\nu}\pi^0$ analysis, and 15 sources are considered in the $p \rightarrow \bar{\nu}\pi^+$ analysis. These can be divided into two classes: those that are common to all SK run periods, and those that depend on the detector geometry of an individual run period. Uncertainties in the nuclear effect cross sections (charge exchange and particle production, absorption, and inelastic scattering) are dominant and are treated as common to all SK run periods. We neglect other common uncertainties such as atmospheric neutrino flux and neutrino interaction cross sections because they are overwhelmed by the nuclear effect uncertainties. Uncertainties in detection efficiency are treated independently for each subsample and run period. The

detection efficiencies for $n \rightarrow \bar{\nu}\pi^0$ nucleon decay signal, for π^0 background, and for muon-induced background in the $p \rightarrow \bar{\nu}\pi^+$ analysis, are taken to have an overall 5% uncertainty due to contributions from detector performance uncertainties, as described in Ref. [6]. The signal and background detection efficiency uncertainties in each decay mode are treated as fully correlated. For $p \rightarrow \bar{\nu}\pi^+$ signal and π^+ -induced backgrounds, the detection efficiency uncertainty is estimated to be larger (15%) due to the possibility that charged pions may interact hadronically as they travel through the water.

The systematic errors that contribute the most to the fits are those from nuclear effects. The cumulative fractions of each category of nuclear effect are shown in Fig. 2 as a function of true π^0 momentum for atmospheric neutrino events (and the corresponding plot for π^+ momentum is similar). We assume an uncertainty of 30% on the cross section for each nuclear effect. As is seen in the figure, charge exchange and absorption effects occur with greater frequency in the momentum range of these decay modes (~ 460 MeV/c). The discontinuity at 500 MeV/c is the result of the transition from the custom simulation used to track pions in the nucleus that are below 500 MeV/c and the GCALOR simulation of pion propagation for pions with momentum equal to or above 500 MeV/c. We anticipate that future SK analyses will model this transition region more completely, but it is well covered by the systematic errors in the current analysis.

The systematic errors used in this analysis and their uncertainties and relative pulls after performing the fitting procedure are shown in Table II. As can be seen in the table, all of the systematic error pulls stay near or below 1σ of their nominal values after the fit, indicating no strong tension between data and MC simulation.

In an unconstrained fit, the best fit value for the β parameter (nucleon decay normalization) falls in the unphysical region for both the $n \rightarrow \bar{\nu}\pi^0$ and the $p \rightarrow \bar{\nu}\pi^+$ analyses, preferring a negative amount of nucleon decay. To avoid this, we constrain the β values to be in the physical region, and determine the 90% confidence level (C.L.) value of β according to the Feldman-Cousins prescription [13]. The partial lifetime lower limit for each decay mode is then calculated according to

$$\tau/\mathcal{B} = \frac{\Delta t \cdot \varepsilon \cdot N_{\text{nucleons}}}{N_{90\text{CL}}}, \quad (2)$$

where \mathcal{B} is the decay mode branching ratio, Δt is the exposure in kton \cdot yrs, ε is the overall signal detection efficiency of the nucleon decay mode, N_{nucleons} is the number of nucleons per kiloton of water (2.7×10^{32} neutrons or 3.3×10^{32} protons), and $N_{90\text{CL}}$ is the number of nucleon decay events allowed at 90% C.L. as determined from the β value.

The physical and unphysical best fit parameter values, signal detection efficiencies for each running period of SK,

TABLE II: Systematic error terms in the $n \rightarrow \bar{\nu}\pi^0$ and $p \rightarrow \bar{\nu}\pi^+$ spectrum fits, with 1σ uncertainties and resulting size of pull terms after fit.

Decay mode	Systematic error	1σ uncertainty (%)	Size of pull after fit (units of σ)
$n \rightarrow \bar{\nu}\pi^0$	Charge exchange + Particle production cross section	30	-1.26
	Pion absorption cross section	30	0.83
	Inelastic scattering cross section	30	-0.42
	SK-I single π^0 BG detection efficiency	5	0.08
	SK-II single π^0 BG detection efficiency	5	-0.19
	SK-III single π^0 BG detection efficiency	5	-0.01
$p \rightarrow \bar{\nu}\pi^+$	Charge exchange + Particle production cross section	30	-0.61
	Pion absorption cross section	30	0.30
	Inelastic scattering cross section	30	-0.12
	SK-I muonic BG detection efficiency 0 decay-e (1 decay-e)	5 (5)	0.01 (0.16)
	SK-II muonic BG detection efficiency 0 decay-e (1 decay-e)	5 (5)	0.00 (0.25)
	SK-III muonic BG detection efficiency 0 decay-e (1 decay-e)	5 (5)	-0.01 (0.18)
	SK-I pionic BG detection efficiency 0 decay-e (1 decay-e)	15 (15)	0.01 (-0.29)
	SK-II pionic BG detection efficiency 0 decay-e (1 decay-e)	15 (15)	0.00 (-0.08)
SK-III pionic BG detection efficiency 0 decay-e (1 decay-e)	15 (15)	0.00 (0.01)	

TABLE III: Best fit parameter values, signal detection efficiency for each SK running period, 90% C.L. value of β parameter, and allowed number of nucleon decay events in the full 172.8 kton \cdot yrs exposure (SK-I: 91.7, SK-II: 49.2, SK-III: 31.9), and lower partial lifetime limit for each decay mode at 90% C.L.

Decay mode	Best fit values (α, β)	Unphysical best fit (α, β)	Signal efficiency (SK-I, -II, -III)%	$\beta_{90\text{CL}}$	Num. signal events at 90% C.L. ($N_{90\text{CL}}$)	τ/\mathcal{B} ($\times 10^{32}$ yrs)
$n \rightarrow \bar{\nu}\pi^0$	(0.940, 0.0)	(0.976, -0.02)	(48.5, 44.0, 48.5)	0.02	19.1	11.0
$p \rightarrow \bar{\nu}\pi^+$	(0.976, 0.0)	(0.996, -0.01)	0-decay-e: (20.4, 23.0, 22.0) 1-decay-e: (14.8, 12.4, 14.2)	0.01	52.8	3.9

and number of nucleon decay events allowed in the data sample at 90% C.L. are shown in Table III. Using the constrained physical best fit parameters and pull terms, the resulting fitted momentum spectra are shown combined for all running periods as the solid black lines in Fig. 3, with the non-observation 90% C.L. allowed amount of signal nucleon decay shown by the hatched histogram and overlaid SK data by black dots. The 90% C.L. partial lifetime lower limits we set for these two decay modes are then $\tau_{n \rightarrow \bar{\nu}\pi^0} > 1.1 \times 10^{33}$ years and $\tau_{p \rightarrow \bar{\nu}\pi^+} > 3.9 \times 10^{32}$ years. In comparison, the predicted range of partial lifetimes allowed for the SO(10) model presented in Ref. [3] are $\tau_{n \rightarrow \bar{\nu}\pi^0} = 2\tau_{p \rightarrow \bar{\nu}\pi^+} \leq 5.7 - 13 \times 10^{32}$ years; the model's allowed ranges are nearly ruled out by the limits presented here. These limits represent an order of magnitude improvement over previously published limits for these two decay modes [14–16] and can be used to more tightly constrain other GUT models that allow these modes.

We gratefully acknowledge cooperation of the Kamioka Mining and Smelting Company. The Super-Kamiokande experiment was built and has been operated with funding from the Japanese Ministry of Education, Science, Sports and Culture, and the United States Department of Energy.

* Deceased.

† Present address: GIST College, Gwangju Institute of Science and Technology, Gwangju 500-712, Korea

‡ Present address: Department of Physics and Astronomy, University of Minnesota, Minneapolis, MN, 55455, USA

- [1] H. Georgi and S. L. Glashow, Phys Rev Lett **32**, 438 (1974).
- [2] J. C. Pati and A. Salam, Phys Rev D **10**, 275 (1974).
- [3] H. Goh, R. Mohapatra, S. Nasri, and S. Ng, Phys Lett B **587**, 105 (2004).
- [4] K. Babu, J. Pati, and Z. Tavartkiladze, JHEP **06**, 1 (2010).
- [5] S. Fukuda et al., Nucl Inst Meth **A** (2003).
- [6] H. Nishino et al., Phys Rev D (2012), hep-ex/1203.4030.
- [7] Y. Hayato, Nucl Phys B Proc Suppl **112**, 171 (2002).
- [8] M. Honda et al., Phys Rev D **75**, 043006 (2007).
- [9] CERN Program Library Long Writeup W5013 (1993).
- [10] Y. Ashie et al., Phys Rev D **71**, 112005 (2005).
- [11] C. Regis et al., Phys Rev D **86** (2012), hep-ex/1205.6538.
- [12] G. L. Fogli, E. Lisi, et al., Phys Rev D **66**, 053010 (2002).
- [13] G. J. Feldman and R. D. Cousins, Phys Rev D **57**, 3873 (1998).
- [14] C. McGrew et al., Phys Rev D **59**, 052004 (1999).
- [15] K. S. Hirata et al., Phys Lett B **220**, 308 (1989).
- [16] D. Wall et al., Phys Rev D **62**, 092003 (2000).

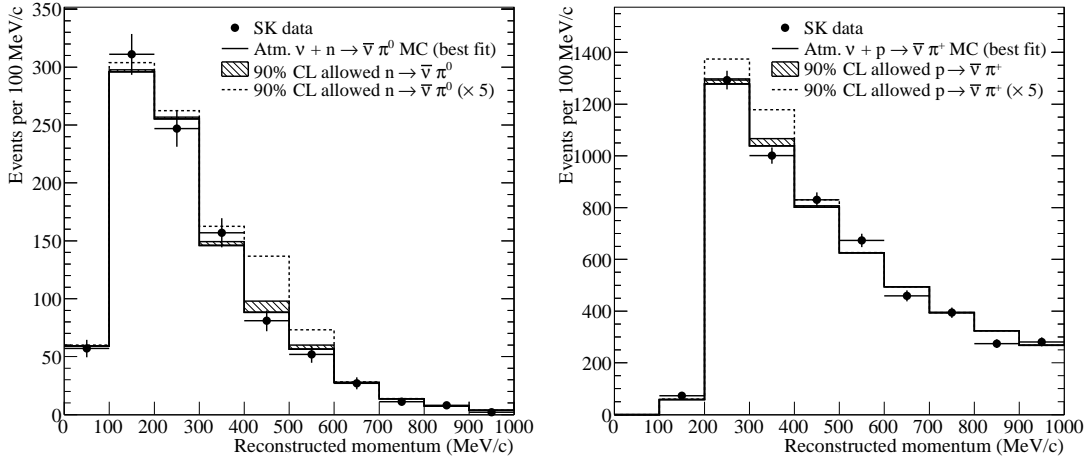


FIG. 3: Reconstructed momentum for 172.8 kton · yrs of SK-I +II+III data (black dots), best fit result of atmospheric neutrino plus nucleon decay MC simulation (solid line), and the 90% C.L. allowed amount of nucleon decay (hatched histogram) for $n \rightarrow \bar{\nu}\pi^0$ (left) and $p \rightarrow \bar{\nu}\pi^+$ (right). The dashed line shows how a positive signal of nucleon decay would look, corresponding to 5 times the limit we set on the decay partial lifetimes. The $p \rightarrow \bar{\nu}\pi^+$ nucleon decay contribution in the right figure is reconstructed at lower momentum than the expected value (458.8 MeV/c) because a muon hypothesis is assumed in the reconstruction.